

Magnetic Amphiphilic Composites Based on Carbon Nanotubes and Nanofibers Grown on an Inorganic Matrix: Effect on Water-Oil Interfaces

Aline A. S. Oliveira,^a Ivo F. Teixeira,^a Leandro P. Ribeiro,^a Juliana C. Tristão,^a
Anderson Dias^b and Rochel M. Lago^{*,a}

^aDepartamento de Química, Universidade Federal de Minas Gerais,
31270-901 Belo Horizonte-MG, Brazil

^bDepartamento de Química, Universidade Federal de Ouro Preto,
35400-000 Ouro Preto-MG, Brazil

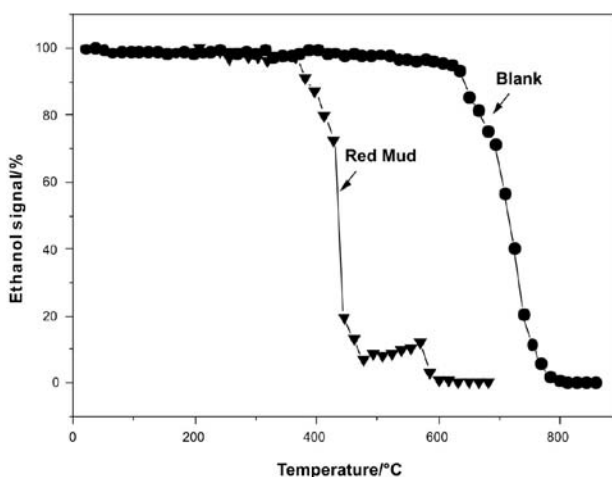


Figure S1. TPCVD profile for the reaction of red mud (RM) with ethanol.

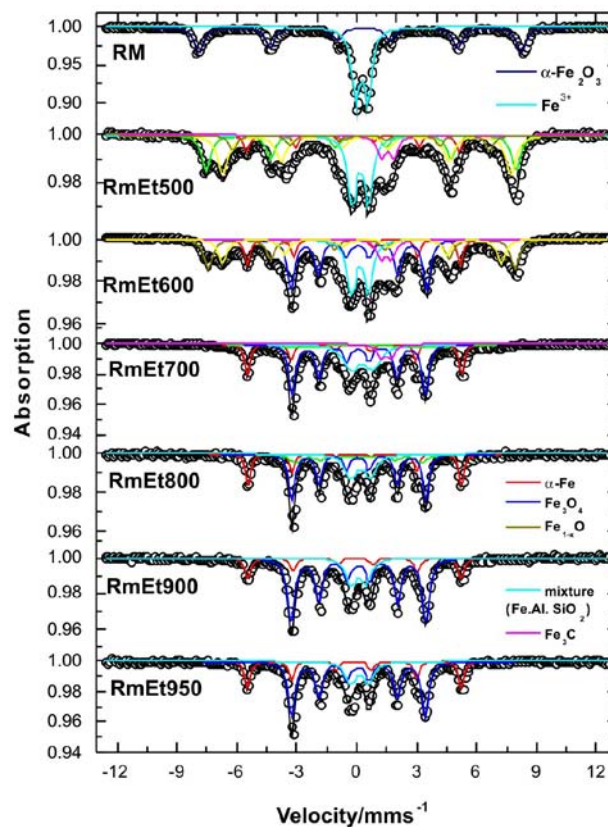


Figure S2. Mössbauer spectra (298 K) registered for pure red mud and the products of TPre (RmEt) at 500, 600, 700, 800, 900 and 950 °C.

*e-mail: rochel@ufmg.br

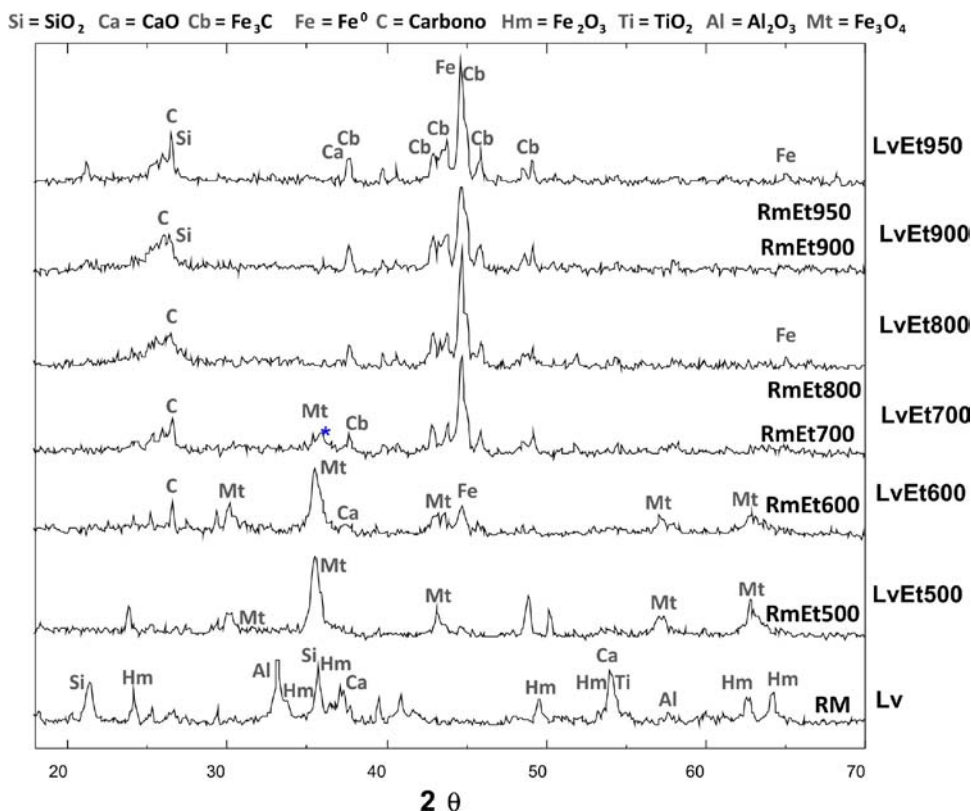


Figure S3. XRD results for RM and the materials prepared at different temperatures.

XRD analyses shown in Figure S3 showed the presence of α -Fe₂O₃, Al₂O₃, CaO, SiO₂ and Ti₂O₃ in the pure red mud.

All prepared materials became strongly magnetic after TPCVD with ethanol with spontaneous magnetization values of 27 to 30 JT⁻¹ kg⁻¹, while the pure red mud presents a magnetization value of 0.7 JT⁻¹ kg⁻¹.

Thermal analyses were also carried out to characterize carbon deposits formed after TPCVD with ethanol. Figure S4 shows TG curves obtained for pure RM and for the samples RmEt700, 800, 900 and 950.

The TG curves showed a mass increase around 300 °C. This increase is likely related to the oxidation of the reduced iron phases which appears in the DTA as an exothermic event. A strong weight loss is also observed from *ca.* 400 up to 500 °C, related to the oxidation of carbon deposits. From these weight losses the carbon content of the composites was estimated. The carbon contents obtained from TG and elemental analyses are shown in Figure 5 in detail. The obtained %C for the samples prepared at 700, 800, 900 e 950 °C were *ca.* 27, 30, 32 and 30%, respectively. The TG derivative curves (Figure S5) showed the presence of enlarged peaks with shoulders in 450 °C, indicating the formation of different forms of carbon, such as amorphous and more organized carbon, *e.g.*, graphitic structures.

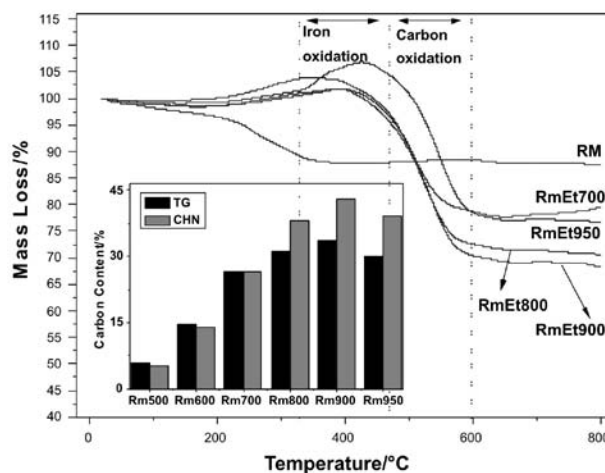


Figure S4. TG curves and carbon contents calculated for the composite materials based on TG and CHN results.

Raman spectra (Figure S6) after reaction with ethanol showed D and G bands at 1380 and 1600 cm⁻¹, respectively. The presence of an intense D band suggests the formation of more defective carbonaceous structures, such as amorphous carbon. On the other hand, a fairly intense G band shows the formation of more organized carbon, such as graphite and carbon nanotubes (CNT). The materials show an asymmetric G peak at *ca.* 1600 cm⁻¹, which suggests the

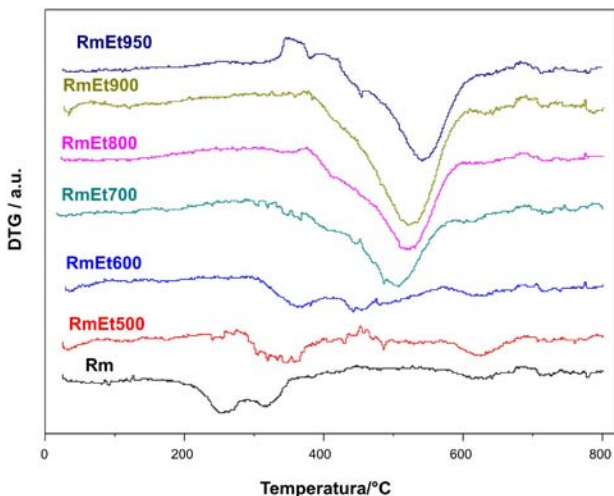


Figure S5. DTG curves for red mud and RmEt500, 600, 700, 800, 900 and 950 composites.

presence of single walled CNT (SWCNT). The G peak of multi-walled CNT (MWCNT) appears at 1580 cm^{-1} , the same position reported for the graphite G band. For the materials prepared at higher temperatures, the G band clearly presents two components. The components known as G+ are related to atomic displacements along the tube axis, and those called G- to modes with atomic displacement along the circumferential direction. A series of bands related to the different oxides, *e.g.*, oxides of Fe, Si, Al and Ti present in the RM, can also be observed in the Raman spectra (range $100\text{--}1800\text{ cm}^{-1}$). Upon reaction with ethanol at 600 °C , no significant change in these bands was noticed. On the other hand, upon reaction at 700 °C new bands at 146 , 170 and 200 cm^{-1} were observed. These bands are likely RBM modes²⁸ related to the formation of single walled carbon nanotubes. These SWCNT present

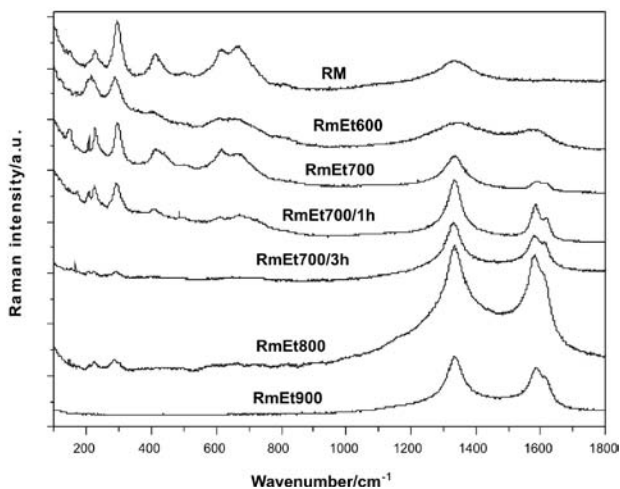


Figure S6. Raman spectra registered for pure red mud (RM) and for the RmEt600, 700, 700/1 h, 700/3 h, 800 and 900 °C samples.

diameters from 1.0 to 1.6 nm , calculated according to the equation $\omega_{\text{RBM}} = 227.0/d_t$.

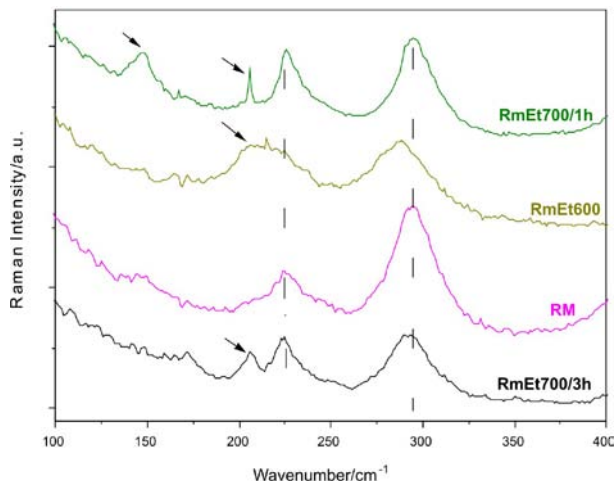


Figure S7. Raman spectra at low frequencies for samples RM, RmEt600, 700/1 h and 700/3 h.

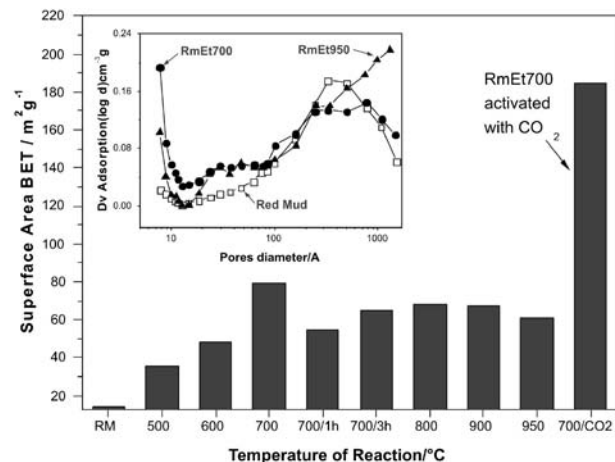


Figure S8. Surface area (BET) values and pore diameters for pure RM and products of TPCVD with ethanol at different temperatures.

The magnetic composites were dispersed in water by sonication for 5 min and the decantation of the particles was followed by a simple measurement of light transmittance in three different wavelengths (450 , 600 and 750 nm). The results are displayed in Figure S9.

It can be observed for pure red mud that the solid particles remained stable in suspension. On the other hand, for the sample RmEt700, a rapid sedimentation was observed, reaching 38% of light retention within *ca.* 10 min. As the TPCVD temperature increased to 800 and 900 °C , the sedimentation rate increased. After *ca.* 15 min all suspensions seemed stable. All the remaining material in suspension was magnetic, and a simple approximation of a magnet removed all particles from the suspension

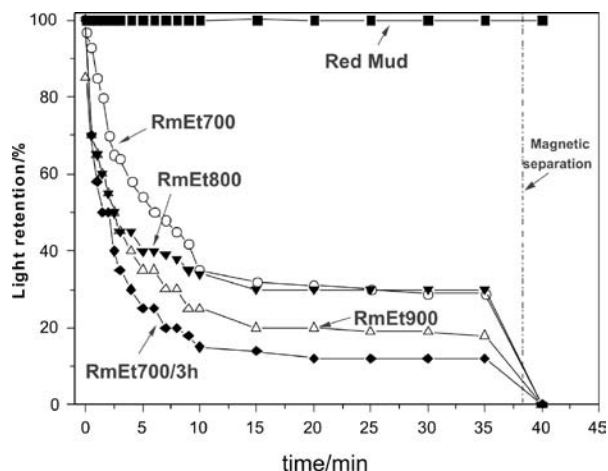


Figure S9. Deposition profile of RM and samples RmEt700, 700/1 h, 800 and 900.

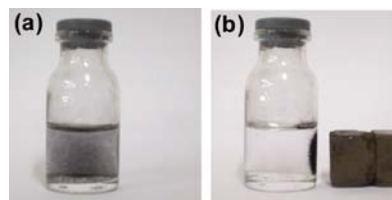


Figure S10. Magnetic particles in suspension (a) and their removal by a magnet (b).

(Figure S10). The amount of suspended particles was obtained by simple separation of the settled material from the suspension after 35 min, followed by drying overnight and weighing. The composites RmEt700, 700/3 h, 800 and 900 showed fractions of particles remaining in suspension of *ca.* 6, 4, 3 and 5 wt%, respectively.

The settled materials were analyzed by SEM and the images are shown in Figure S11.

Figure S11 suggests that ethanol TPCVD produced

large amount of filamentous carbon in all samples obtained above 700 °C. The carbon filaments are in average 20 μm long with diameters varying from 10 up to 100 nm. EDS analysis after CVD showed the presence of different metals with a high concentration of carbon (Figure S12).

After dispersion in water, the material remaining in suspension was analyzed by SEM, showing aggregates of particles of 100-300 nm diameter and carbon filaments (Figure S13).

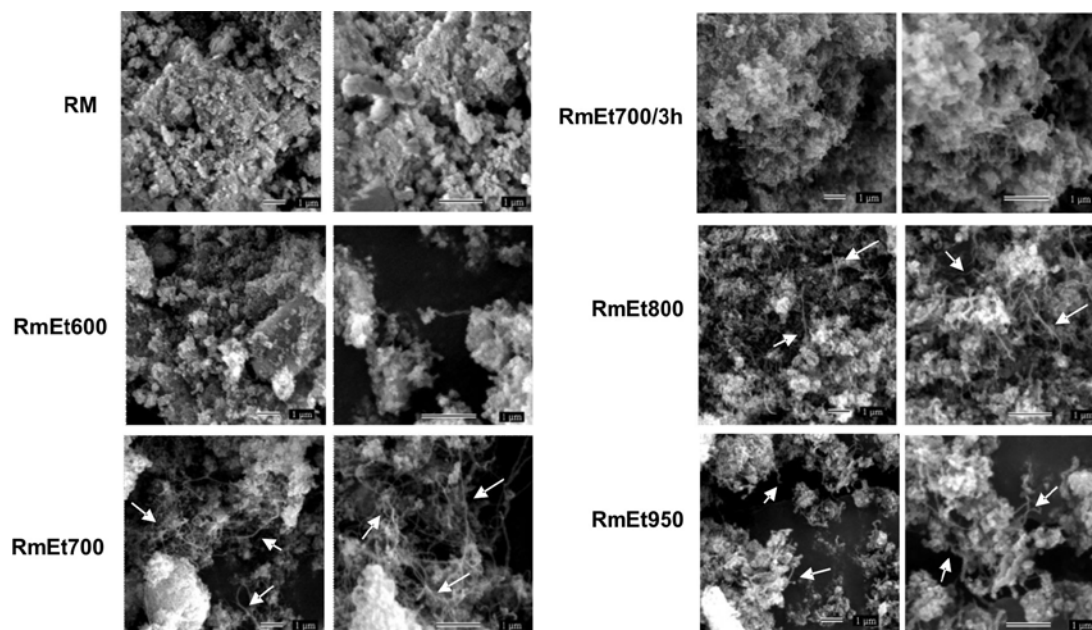


Figure S11. SEM images of RM and the magnetic composites after dispersion and settling in water.

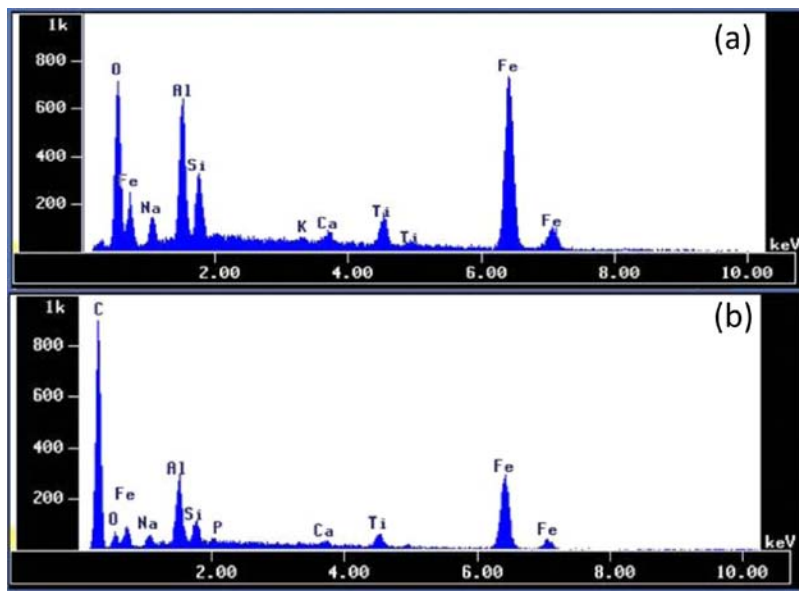


Figure S12. EDS microanalysis of (a) pure RM and (b) RmEt900.

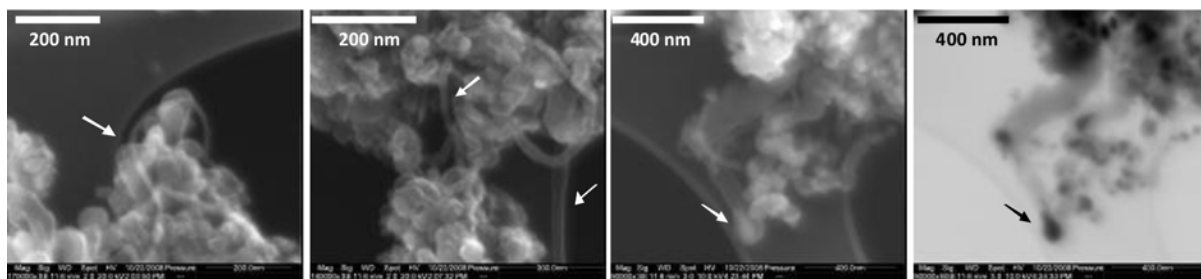


Figure S13. SEM images of the suspended material in sample RmEt700.

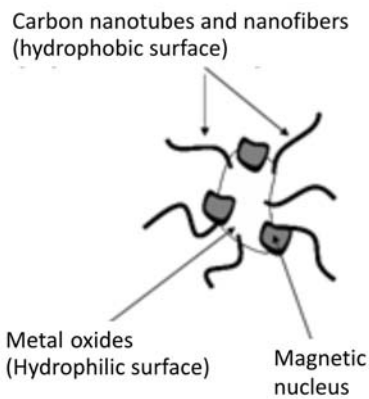


Figure S14. Scheme of the nanostructured, amphiphilic magnetic composite obtained from RM.

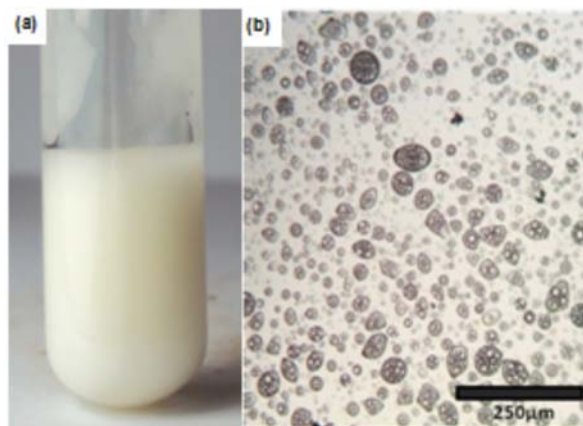


Figure S15. Emulsion of water 30% v/v in biodiesel, (a) macro and (b) microscopic aspect.

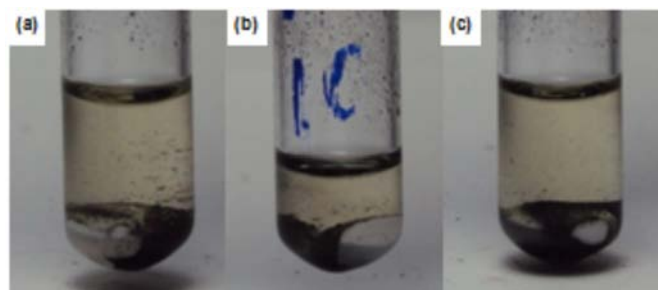


Figure S16. Images obtained after a demulsification test carried out for (a) RmEt600, (b) RmEt700 and (c) RmEt700/1 h, with 1000 ppm of the composites.

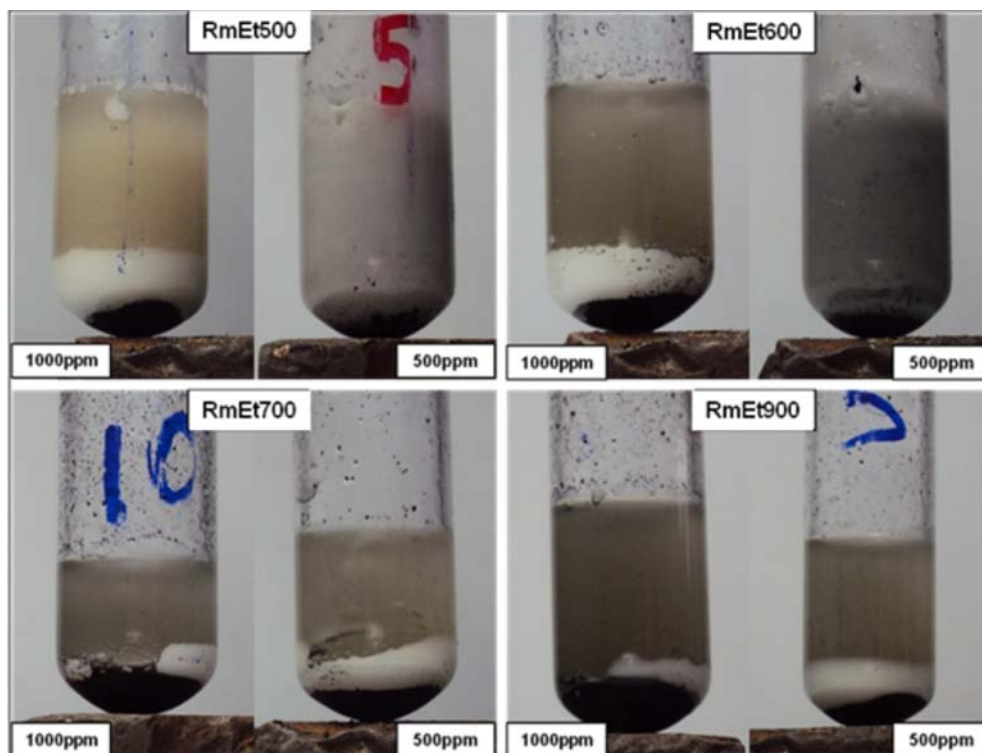


Figure S17. Emulsions with 1000 and 500 ppm of RmEt 500, 600, 700 and 900 after exposure to a magnetic field for 5 min.

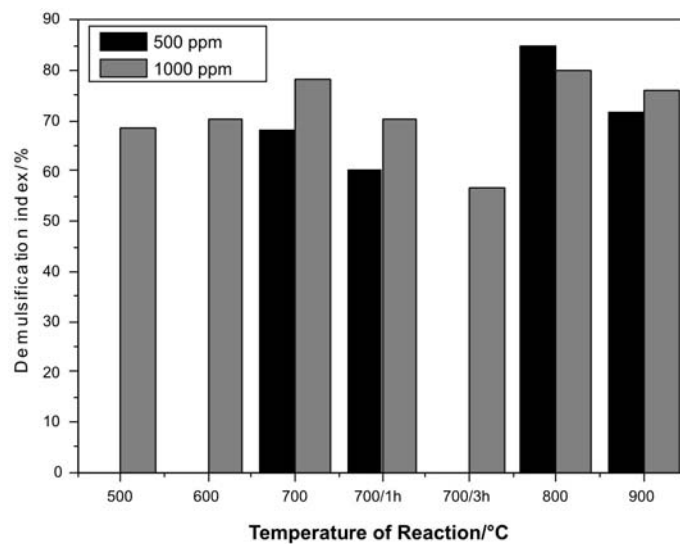


Figure S18. Demulsification index for the biodiesel/water emulsion with the composite described in this work. $DI = (\text{Demulsified Layer Height}/\text{Overall Height}) \times 100$.

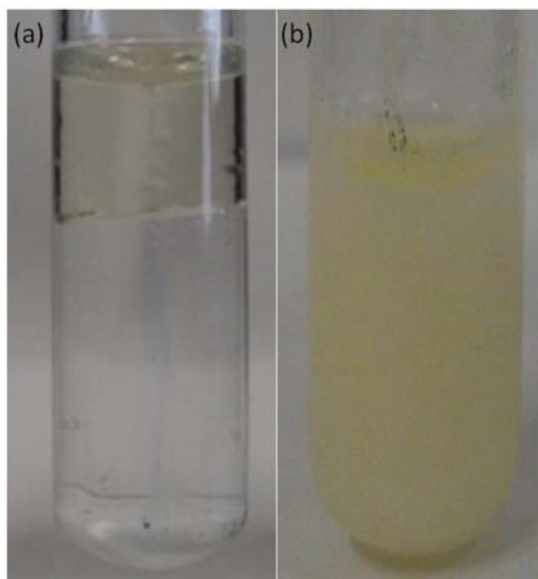


Figure S19. Macroscopic aspect of (a) water/soybean oil mixture and (b) stable emulsion formed with the emulsifier described in this work.

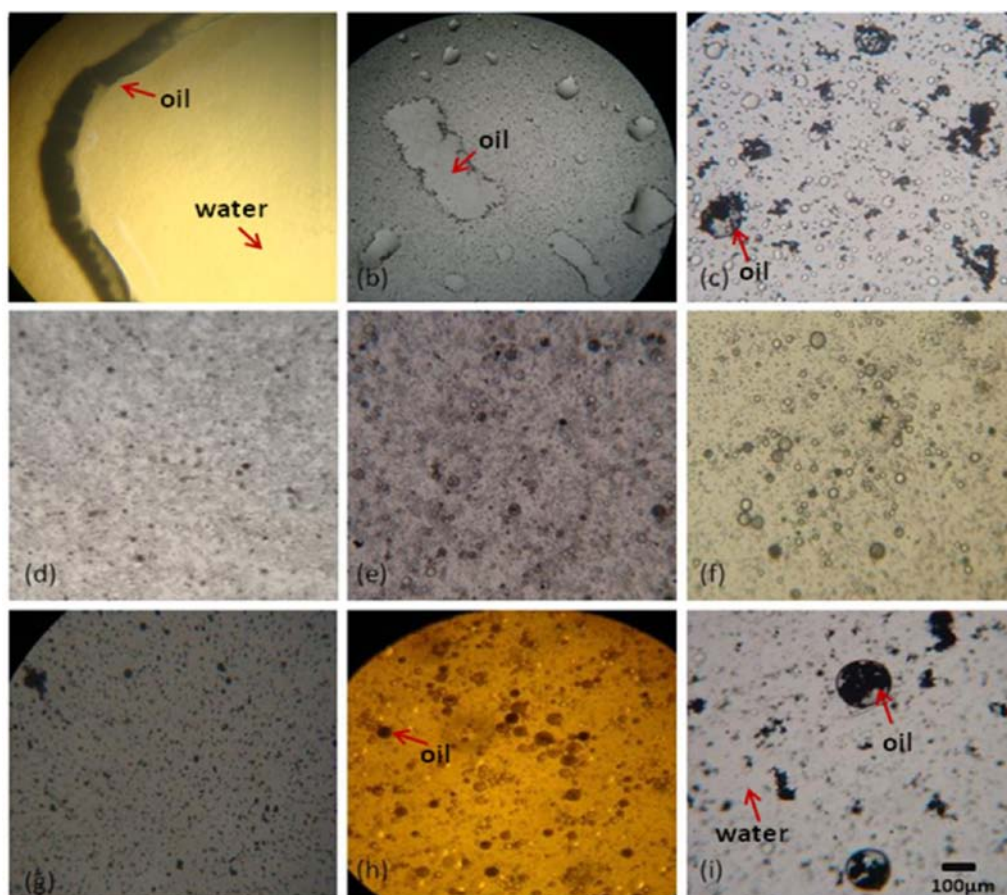


Figure S20. Microscopic images of (a) water and oil mixture and (b)-(i) emulsions formed with the amphiphilic composites prepared from red mud at different temperatures: (b) 500, (c) 600, (d) 700, (e) 700/1 h, (f) 700/3 h, (g) 800, (h) 900 and (i) 950 °C.

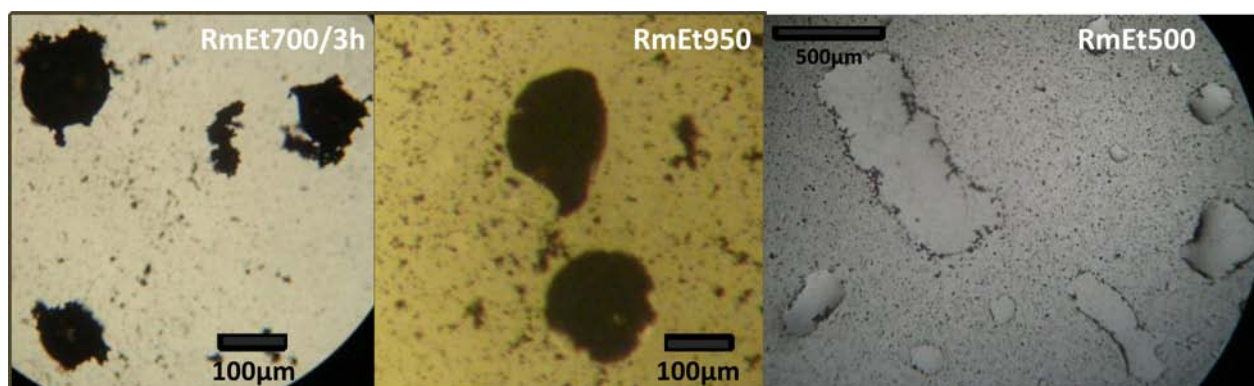


Figure S21. Different interactions of samples RmEt700/3 h, 950 and 500 on the oil/water interface.

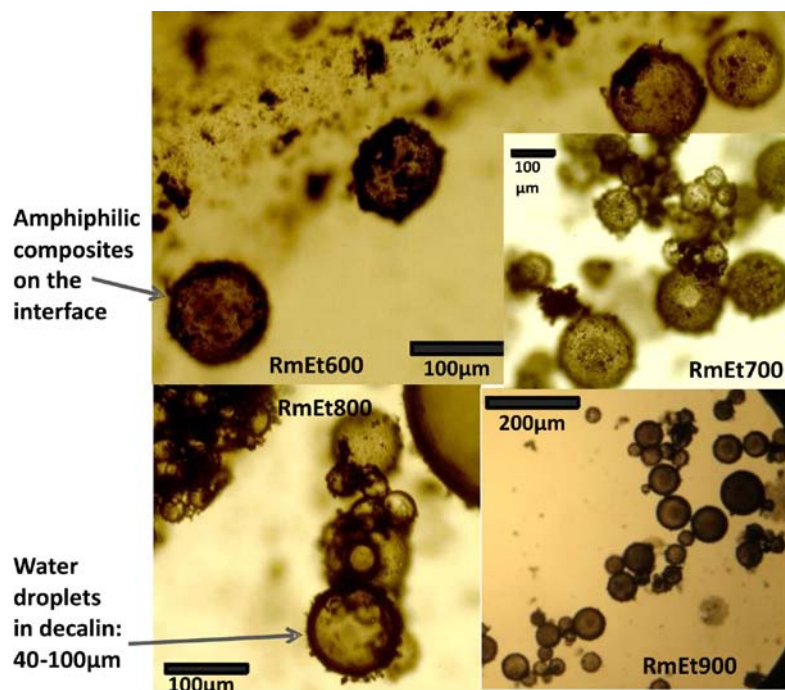


Figure S22. Microscopic images of emulsions formed with the amphiphilic composites prepared from RM at different temperatures: 600, 700, 800 and 900°C.

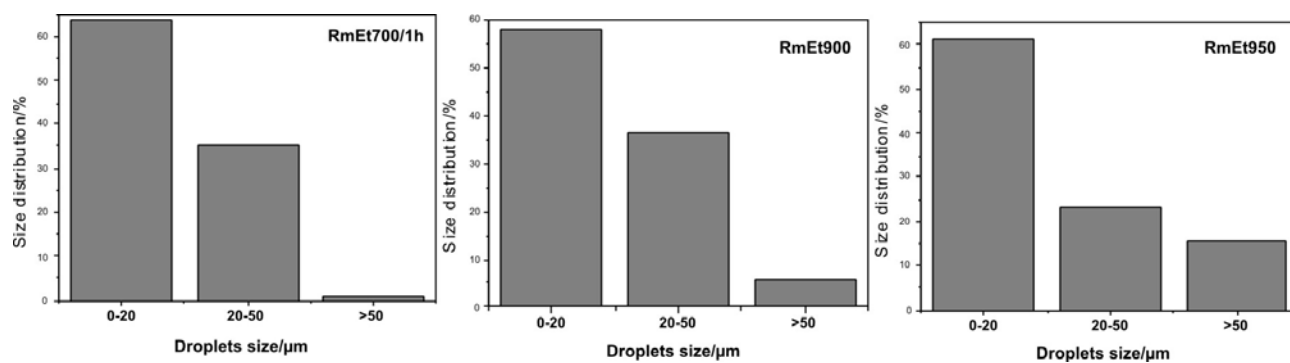


Figure S23. Droplet size distribution for emulsions formed by samples RmEt 700/1 h, 900 and 950.